Heterologous Expression of Human Norovirus GII.4 VP1 Leads to Assembly of T=4 Virus-Like Particles

Jessica Devant[1,2], Götz Hofhaus[3], David Bhella[4], and Grant S. Hansman[1,2,#]

[1]Schaller Research Group at the University of Heidelberg and the DKFZ, Heidelberg, Germany

[2]Department of Infectious Diseases, Virology, University of Heidelberg, Heidelberg, Germany

[3]Bioquant, CellNetWorks, University of Heidelberg, Heidelberg, Germany

[4]MRC, University of Glasgow Centre for Virus Research, Glasgow, Scotland

SHORT TITLE: Cryo-EM structure of GII.4 norovirus VLPs

[#]Corresponding author

Grant S. Hansman: CHS Foundation, University of Heidelberg, and German Cancer Research Center, Heidelberg, Germany. Email: g.hansman@dkfz.de

ABSTRACT

Human noroviruses are a leading cause of acute gastroenteritis, yet there are still no vaccines or antivirals available. Expression of the norovirus capsid protein (VP1) in insect cells typically results in the formation of virus-like particles (VLPs) that are morphologically and antigenically comparable to native virions. Previous structural analysis of norovirus VLPs showed that the capsid has a T=3 icosahedral symmetry and is composed of 180 copies of VP1 that are folded into three quasi-equivalent subunits (A, B, and C). In this study, we determined the cryo-EM VLP structures of two GII.4 variants, termed CHDC-1974 and NSW-2012. Surprisingly, we found that greater than 95% of these GII.4 VLPs were larger than virions and 3D reconstruction showed that these VLPs exhibited T=4 icosahedral symmetry. We found that the T=4 VLPs showed several structural differences to the T=3 VLPs. The T=4 particles assemble from 240 copies of VP1 that adopt four quasi-equivalent conformations (A, B, C, and D) that form two distinct dimers, A/B and C/D. The T=4 protruding domains were elevated ~21-Å off the capsid shell, which was ~7-Å more than the previously studied GII.10 T=3 VLPs. A small cavity and flap-like structure at the icosahedral twofold axis disrupted the contiguous T=4 shell, a consequence of the D-subunit S-domains having smaller contact interfaces with neighboring dimers. Overall, our findings that old and new GII.4 VP1 sequences assemble T=4 VLPs might have implications for the design of potential future vaccines.

39 IMPORTANCE

40

41 The discovery that the GII.4 VLPs have a T=4 symmetry is of significance, since this
42 represents the first known T=4 calicivirus structure. Interestingly, the GII.4 2012
43 variant shares 96% amino acid identity with a current GII.4 VLP vaccine candidate
44 sequence, which suggests that this vaccine might also have a T=4 symmetry. Our
45 previous results with these GII.4 VLPs showed functional binding properties to
46 antibodies and Nanobodies that were raised against T=3 (GII.10) VLPs. This suggests
47 that the T=4 VLPs were antigenically comparable to T=3 particles, despite the
48 obvious structural and size differences. On the other hand, these larger T=4 VLPs
49 with novel structural features and possibly new epitopes might elicit antibodies that
50 do not recognize equivalent epitopes on the T=3 VLPs. Further structural and binding
51 studies using a library of GII.4-specific Nanobodies are planned in order to precisely
52 investigate whether new epitopes are formed.

INTRODUCTION

Human noroviruses are members of the *Caliciviridae* family and are a leading cause of outbreaks of acute gastroenteritis. The virus has a positive sense, single stranded RNA genome of ~7.7 kbp. The genome is organized into three open reading frames (ORFs), where ORF1 encodes nonstructural proteins and ORF2 and ORF3 encode a major structural protein (termed VP1) and a minor structural protein (termed VP2), respectively. Noroviruses are genetically diverse and based on VP1 sequences have been classified into seven genogroups (GI-GVII), where GI, GII, and GIV cause infections in humans (1, 2). The GI and GII are further subdivided into numerous genotypes, with GII genotype 4 (GII.4) recognized as the most prevalent and clinically important strain (3, 4).

Recently, two human norovirus cell culture systems were developed (5, 6). However, mechanistic studies of norovirus structure and biology, such as interaction with the host receptor(s), remain challenging owing to difficulties in preparing large-scale virion preparations. Expression of ORF2 alone in insect or mammalian cells can result in the formation of virus-like particles (VLPs) that are antigenically and morphologically similar to native virions (2, 7-10). Expression of norovirus VLPs has permitted studies on host binding factors, interactions with norovirus-specific antibodies, and structural studies (2, 11-16). Indeed, histo-blood group antigens (HBGAs) and bile acids were shown to be important binding co-factors for human norovirus VLPs and/ or virions (17-22).

77 Structural analysis of GI.1 VLPs revealed that VP1 is separated into two distinct
78 domains: a shell domain (S domain) that encloses the RNA and a protruding domain
79 (P domain) that binds to co-factors, such as HGBAs and bile acids (8, 19, 21). A
80 hinge region, which is typically composed of 10-14 amino acids, connects the S and P
81 domains. The P domain has a β-barrel fold that is structurally conserved in the
82 *Caliciviridae* family. Dimerization of the P domains forms arch shaped protrusions
83 that are visible in electron microscopy images. The P domain is further subdivided
84 into P1 and P2 subdomains, where the P2 subdomain is an insertion in the P1
85 subdomain and is the most variable region on the capsid (8).
86
87 Structural studies have shown that caliciviruses have a common overall organization
88 of T=3 icosahedral symmetry and are comprised of 180 copies of VP1 (7, 8, 23-25).
89 Within the asymmetric unit, VP1 adopts three quasi-equivalent conformations, termed
90 A, B, and C (8). The norovirus A and B subunits assemble into 60 dimers (termed
91 A/B) at the quasi twofold axis, whereas the C subunits assemble into 30 C/C dimers
92 that are located at the strict icosahedral twofold axis. For the GI.1 VLPs, the A/B
93 dimers have a convex S domain conformation, whereas the C/C dimers have a flat S
94 domain conformation (8). The conformational differences within these dimers likely
95 facilitates the curvature of the virus particle to form a closed shell, such features are
96 commonly seen in other T=3 icosahedral viruses (26). Interestingly, smaller norovirus
97 VLPs (~25 nm in diameter) that are assumed to have a T=1 icosahedral symmetry
98 have also been reported (22, 27); however to date, structures of these smaller VLPs
99 have not been published.
100

Here, we show the cryo-EM structures of VLPs for two GII.4 variants that were identified in 1974 and 2012, termed CHDC-1974 and NSW-2012, respectively (15, 28). We show that these VLPs have a T=4 icosahedral symmetry and are composed of 240 copies of VP1. In order to form the T=4 icosahedral structure, VP1 adopts four quasi-equivalent conformations, termed A, B, C, and D, giving rise to two distinct types of dimers, termed A/B and C/D. The VLPs consisted of 60 A/B dimers and 60 C/D dimers, with B, C, and D subunits located at the twofold axis, and the A subunit at the fivefold axis. As GII.4 VLPs are currently under consideration as vaccine candidates, our findings might have implications with respect to the likely antigenic properties of such assemblies.

MATERIALS AND METHODS

VLP and virion preparation

The NSW-2012 and CHDC-1974 VLPs (Genebank accession numbers JX459908 and ACT76142, respectively) were expressed in a baculovirus system as previously described (29-31). Briefly, the bacmid containing the recombinant VP1 gene was transfected in Sf9 insect cells. After incubation for five days, the culture medium was centrifuged for 10 min at 3,000 rpm at 4°C. The recovered baculovirus was subsequently used to infect Hi5 insect cells. At five days post infection, the culture medium was centrifuged for 10 min at 3,000 rpm at 4°C and then 1 h at 6,500 rpm at 4°C. The VLPs in the supernatant were concentrated by ultracentrifugation at 35,000 rpm (Beckman Ti45) for 2 h at 4°C and then further purified using CsCl equilibrium gradient ultracentrifugation at 35,000 rpm (Beckman SW56) for 18 h at 4°C. To remove the CsCl, the VLPs were pelleted for 2 h at 40,000 rpm (Beckman TLA55) at 4°C and subsequently resuspended in PBS (pH 7.4). GII.4 virions in stool were also purified using this centrifugation technique, except for the CsCl gradient step.

Negative stain electron microscopy

The integrity of the VLPs was confirmed using negative stain electron microscopy (EM). The VLPs were diluted 1:30 in distilled water and applied to EM grids. The grids were washed with distilled water, stained with 0.75% uranyl acetate, and the excess uranyl acetate was removed with filter paper. Virion samples were applied to EM grids, washed with water, fixed with 4% glutaraldehyde, and then stained as above. EM images were acquired on a Zeiss 910 electron microscope at 50,000× magnification.

136

137 **Cryo-EM data sample preparation and data collection**

138 UNSW-2012 and CHDC-1974 VLPs (3 µl) were applied to freshly glow discharged
139 Quantifoil holey carbon support films (R1.2/1.3) and blotted for 18 seconds at 100%
140 humidity and 10°C before being plunged in liquid ethane using an FEI Mark IV
141 Vitrobot (Thermo Fischer Scientific). Vitrified specimens were imaged on a Titan
142 Krios microscope (Thermo Fisher scientific) operated at 300 keV. NSW-2012
143 micrographs were acquired with a K2 direct electron detector with Latitude S
144 software (Gatan) at 64,000× magnification corresponding to a pixel size of 2.27 Å/px,
145 while CHDC-1974 micrographs were collected using a K3 direct electron detector at
146 64,000× magnification, corresponding to a pixel size of 1.375 Å/px.

147

148 **Cryo-EM data processing**

149 Initially, the movies containing 16 frames for NSW-2012 and 40 frames for CHDC-
150 1974 were motion corrected using motioncor2 software (32) and defocus estimation
151 was performed using ctffind 4.1 software (33). All further image-processing steps
152 were performed using Relion 2.1 software for NSW-2012 and cryoSPARC software
153 for CHDC-1974 (34, 35). An initial set of 1,000 particles was manually picked for 2D
154 classification to produce averages suitable as references for automated particle
155 picking. The autopicked particles were sorted in a 2D classification step and the best
156 particles were used for calculation of an initial starting model, followed by 3D
157 classification. A subset of particles that generated the highest resolution was selected
158 for further refinement. The 3D refinement and post-processing of NSW-2012 from
159 10,548 T=4 particles produced a final map at 7.3-Å resolution with icosahedral (I2)
160 symmetry imposed (0.143 FSC cutoff). Smaller NSW-2012 T=3 particles were

161 manually picked and sorted in 2D classification. In total, 391 particles were selected
162 for further 3D structure determination. Refinement of these smaller NSW-2012 T=3
163 particles yielded a map of 15-Å resolution. For CHDC-1974, a subset of 42,485
164 particles for refinement led to the calculation of a map at 6.1-Å resolution using the
165 0.143 FSC cutoff. Cryo-EM T=4 VLP structures for CHDC-1974 (accession number:
166 EMD-4549) and NSW-2012 (EMD-4550) were deposited at EMDB. The cryo-EM
167 VLP structure for NSW-2012 with T=3 icosahedral symmetry is available on request.
168
169 **Fitting of the X-ray structures into the density maps**
170 Crystal structures of NSW-2012 P domain (4OOS) and CHDC-1974 P domain
171 (5IYN) were fitted into the respective densities using the "fit in map" command in the
172 UCSF Chimera software (36). Since a high-resolution GII.4 shell domain structure
173 was unavailable, the GI.1 Norwalk virus S domain was extracted from the X-ray
174 crystal structure (1IHM) and fitted into the GII.4 cryo-EM densities using UCSF
175 Chimera software.

RESULTS AND DISCUSSION

The purpose of this study was to analyze GII.4 VLP architecture and compare these assemblies to the previously solved GI.1 and GII.10 VLP structures. The NSW-2012 VP1 sequence had a single amino acid insertion at position ~394 (NSW-2012 numbering) compared to CHDC-1974 (Fig. 1). Overall, NSW-2012 and CHDC-1974 shared 89% amino acid identity, with most (45 of 54) amino acid substitutions occurring in the P domain. Negative stain EM images revealed that the VLPs exhibited characteristic norovirus morphology (Fig. 2). However, the diameter of these VLPs was measured to be ~52 nm, which suggested that the GII.4 VLPs were larger than GII.10 and GI.1 VLPs that had diameters of ~43 nm and ~38 nm, respectively.

Cryo-EM structure of NSW-2012 T=4 VLPs

The structure of the NSW-2012 VLPs was determined using cryo-EM and 3D icosahedral image reconstruction. The VLPs were mono-disperse in vitreous ice and appeared mostly homogenous in size (Fig. 3A). From the 364 images, 10,548 particles were used for image reconstruction and refined to 7.3-Å resolution (Fig. 3C). Unexpectedly, NSW-2012 VLPs were discovered to have T=4 icosahedral symmetry (Fig. 4). Our data revealed that these VLPs were composed of 240 copies of VP1, rather than 180 VP1 copies as in GI.1 and GII.10 VLPs. The inner diameter of NSW-2012 shell was measured as 32 nm, while the outer capsid diameter was 50 nm. The larger diameter of the T=4 VLPs corresponded to a capsid volume of ~12,724 nm^3, which was ~2.1 times the volume of the GII.10 VLPs that had an inner diameter of 23 nm, corresponding to a volume of ~5,985 nm^3 (7).

Another interesting structural feature of these NSW-2012 VLPs was a small cavity and flap-like structure on the contiguous shell (Fig. 5). This feature was associated with the S domain and found on opposing sides at the twofold axis. This feature may arise as a consequence of the C/D dimer having a stronger curvature, preventing the S-domain from forming the expected contacts with neighboring B and C-type subunits. Alternatively, there might be insufficient space to allow the D subunit S-domain to pack, such that it lies in the plane of the shell without causing steric collision with neighboring subunits.

Structural analysis of the T=4 VLPs indicated that VP1 adopted four quasi-equivalent conformations, termed A, B, C, and D. These four subunit conformations formed two distinct dimer classes: A/B and C/D (Figs. 4 and 6). The B, C, and D subunits alternated about the two-fold symmetry axis, while the A subunit was positioned at the fivefold axis (Fig. 4). The T=4 VLPs were composed of 60 A/B dimers and 60 C/D dimers, which was distinct from the T=3 VLPs that have been shown to be assembled from 60 A/B and 30 C/C dimers. We also observed that both A/B and C/D dimers had a convex S domain conformation, which was in contrast to the GI.1 VLPs that consisted of both convex (A/B) and flat (C/C) dimers (8).

In order to better comprehend how VP1 assembled into the T=4 VLPs, the X-ray crystal structure of NSW-2012 P domain (4OOS) and GI.1 S domain (1IHM) were fitted into the VLP density map. We found that the NSW-2012 P domain dimer could be unambiguously positioned into the VLP density, with a cross correlation coefficient of 0.96 (Fig. 7A). This result indicated that the P domain dimers on the

T=4 VLPs had not undergone any major structural modifications. In the case of the S domain, the GI.1 S domain needed to be manually positioned into the density map. The GI.1 S domain fitted well into to A/B dimer and the C subunit, while the D subunit needed to be further repositioned (Fig. 7B). This additional fitting in the D subunit was necessary in order to occupy the elevated density of the flap-like regions.

Unfortunately, it was problematic to fit the hinge region, since the hinge region on the X-ray crystal structure of NSW-2012 P domain was excluded from the expression construct and the hinge region of the GI.1 VLPs was flattened (7, 8). Interestingly, an apparent point of contact was also observed between the S domain and the C-terminus of the P domain on the D subunit (Fig. 8). This may stabilize the convex conformation of the C/D dimer and possibly the T=4 VLPs. Indeed, the C-termini of VP1 on the GI.1 VLPs and the GII.4 P domain were found to be flexible (8, 37). Moreover, the C-terminus of VP1 was previously shown to be important for the size and stability of VLPs (38).

Another interesting feature that we observed with the T=4 VLPs was the raised P domains (Figs. 4 and 8). We found that the T=4 P domain was elevated ~21-Å off the shell by an extended hinge region, which was higher than the P domains on the GII.10 VLPs, which were raised ~14-Å (7). The hinge region in NSW-2012 and GII.10 (7) were both ~10 amino acids and mainly conserved (39). This result suggested that the raised P domains might be a structural feature of GII noroviruses, since the P domains on the GI.1 VLPs were essentially resting on the shell (8).

Cryo-EM structure of NSW-2012 T=3 VLPs

To determine the structure of a recent GII.4 isolate (NSW-2012), 10,548 particles were imaged by cryo-EM, and a 3D image reconstruction was calculated. Unexpectedly, this analysis revealed a previously unknown T=4 assembly. In this preparation however, a very small number of particles (391 particles) appeared smaller (~46 nm) than the ~50 nm VLPs (Fig. 4A). Reconstruction of these particles at ~15-Å resolution revealed the expected T=3 icosahedral symmetry (Fig. 9). At this resolution, the hinge region was not visible. Also, the cavity and flap-like structures that characterized the T=4 VLP were not present. Based on the T=3 geometry, these VLPs were likely composed of 180 copies of VP1, however the VP1 dimers or subunits were not clearly resolved. Overall, these results indicated that NSW-2012 VP1 formed VLPs of which ~5% of the population (391 of 10,548) were T=3 particles. This proportion was confirmed over several VLP preparations. Unfortunately, owing to the low numbers it remains challenging to improve on the achieved resolution, since only few T=3 VLPs were expressed and were not able to be separated from the T=4 VLPs using CsCl or sucrose gradient ultracentrifugation.

Cryo-EM structure of GII.4 CHDC-1974 T=4 VLPs

To test whether assembly of VLPs with T=4 icosahedral symmetry is a property of VP1 from all GII.4 strains, we proceeded to determine the cryo-EM structure of VLPs produced by VP1 of CHDC-1974. The VLPs were mostly mono-disperse and homogenous in size (Fig. 10A). From 591 images, 42,485 particles were processed to calculate a reconstruction with a final resolution of 6.1-Å (Fig. 10B). The CHDC-1974 VLPs also had T=4 symmetry (Fig. 11) and their structure closely resembled that of NSW-2012 VLPs. Unlike NSW-2012 however, CHDC-1974 VP1 only assembled into T=4 VLPs and no T=3 VLPs were identified.

We found that CHDC-1974 T=4 VLPs were also composed of 240 copies of VP1 that formed the quasi-equivalent subunits A, B, C, and D and A/B and C/D dimeric capsomeres. The inner diameter of the shell was 32 nm, whereas the outer diameter of the capsid was 50 nm. As in NSW-2012 VLPs, cavity and flap-like structures were also present on the CHDC-1974 VLPs (Fig. 12). The CHDC-1974 A/B and C/D dimers showed a similar convex conformation as NSW-2012 dimers, although slightly less pronounced (Fig. 13). The X-ray crystal structure of CHDC-1974 P domain (5IYN) was easily fitted into the CHDC-1974 VLP density map (Fig. 14A). The GI.1 S domain also fitted into the A, B, and C subunits, whereas the GI.1 S domain was repositioned to occupy the D subunit density (Fig. 14B). Similar to NSW-2012 VLPs, a possible contact interface was observed between the S and P domains on the D subunit (Fig. 15). Lastly, we found that CHDC-1974 P domain was also lifted off the shell ~21-Å by an extended hinge region (Figs. 11 and 15).

Overall, these results showed that GII.4 VP1 sequences isolated over three decades apart remained structurally conserved. This could imply that other GII.4 VP1 sequences would also form T=4 VLPs when expressed in insect cells, especially since these two sequences had only 89% amino acid identity.

Previous binding studies using GII.4 capsids

GII.4 VLPs and their corresponding P domains have been extensively examined for binding to co-factors (HBGAs and bile acid), antibodies, human milk oligosaccharides (HMOs), and Nanobodies (21, 31, 37, 39-41). NSW-2012 P domains were capable of binding numerous HBGA types and the VLPs cross-reacted with

Nanobodies and antibodies that were raised against other genotypes or GII.4 variants. However, the NSW-2012 VLPs did not bind bile acid and poorly bound HMOs (unpublished). Overall, these results suggested that T=4 VLPs were indeed antigenically relevant and capable of functioning similarly to GII.4 virions with respect to antigenicity and HBGA interactions.

GII.4 VLPs in vaccine trials

VLP vaccines against norovirus that are currently in clinical trials use a combination of GI.1 VLPs and modified GII.4 VLPs (termed GII.4c) (42, 43) Negative stain EM images of these GII.4c VLPs showed the typical norovirus morphology. However, the size determination and the structure are not available. Interestingly, GII.4c and NSW-2012 shared 94% amino acid identity with most substitutions (28 of 31) located in the P domain (Fig. 1). Therefore, it is tempting to speculate that GII.4c VP1, which closely matched NSW-2012 VP1 sequence, might also form T=4 VLPs particles. In both VLPs, VP2 is not present.

To test whether GII.4 virions are T=3 or T=4 assemblies, we used negative stain EM of authentic GII.4 virions. These virion images revealed a smaller diameter of ~44 nm compared to the T=4 VLPs (~50 nm) (Fig. 16). This size corresponds to the diameter determined for the NSW-2012 T=3 VLPs and indicates that GII.4 virions likely exhibit T=3 icosahedral symmetry.

In general, studies have shown that norovirus-specific antibody titers were raised after vaccination with VLPs, but the levels of protection were not strongly improved compared to placebo groups (44). This might indicate that vaccination leads to

326 production of neutralizing antibodies against epitopes on T=4 VLPs that are not
327 accessible on T=3 virions (i.e., when challenged) and that therefore vaccine efficacy
328 could be lowered by a sub-optimal antigen. Clearly, further studies are needed in
329 order to determine whether the GII.4c VLPs form T=4 particles and if the T=4 VLPs
330 are antigenically identical to T=3 VLPs.
331
332 **Summary**
333 We have shown that upon heterologous expression of human norovirus GII.4 VP1 in
334 insect cells, VLPs are formed that adopt T=4 icosahedral symmetry. This is at odds
335 with the likely T=3 symmetry virions encoded by this virus. There are two important
336 consequences of this outcome. Firstly, the assembly of GII.4 T=4 VLPs may impact
337 on results from previous studies in which it was assumed that GII.4 norovirus VLPs
338 were morphologically similar to virions. Secondly, the cavity and flap-like structures
339 on the T=4 could elicit antibodies that are not capable of recognizing T=3 virions.
340 Further structural and binding studies using a library of GII.4-specific Nanobodies are
341 planned in order to investigate these novel epitopes.

342 ACKNOWLEDGEMENTS

343

344 We acknowledge the excellence cluster CellNetworks (Cryo-EM network) of the
345 University of Heidelberg for cryo-EM data collection, the EM core facility at DKFZ,
346 and Baden-Württemberg High Performance Cluster (bwHPC). We thank Anna
347 Koromyslova for EM images of GII.4 virions and Benedikt Wimmer for setting up the
348 cryo-EM software. The funding for this study was provided by the CHS foundation;
349 the Baden-Württemberg Stiftung (GLYCAN-BASED ANTIVIRAL AGENTS);
350 Deutsche Forschungsgemeinschaft (DFG, FOR2327); and the BMBF VIP+ (Federal
351 Ministry of Education and Research) (NATION, 03VP00912).

352 FIGURE LEGENDS

353

354 **Figure 1. Amino acid sequence alignment of GII.4 VP1.** NSW-2012 (JX459908),
355 CHDC-1974 (ACT76142), and GII.4c (42) VP1 amino acid sequences were aligned
356 using ClustalX. The S domain (orange), hinge region (green), P1 subdomain (light
357 blue), and P2 subdomain (navy) were labeled accordingly. Compared to CHDC-1974,
358 NSW-2012 and GII.4c VP1 had a single amino acid insertion (arrow) at position 394
359 (NSW-2012 numbering). The S domain and hinge region were mainly conserved,
360 whereas most amino acid substitutions were located in the P2 subdomain.

361

362 **Figure 2. EM images of GI and GII VLPs.** Negative stain EM images of norovirus
363 VLPs show the characteristic norovirus virion morphology (50,000× magnification).
364 The diameter of the CHDC-1976 and NSW-2012 VLPs was ~52 nm, whereas the
365 diameter of GI.1 West Chester (AY502016.1) and GII.10 Vietnam026 (AF504671)
366 VLPs were ~38 nm and ~43 nm, respectively (45, 46). The bar represents 100 nm.

367

368 **Figure 3. NSW-2012 cryo-EM data processing.** (A) A representative cryo-EM
369 micrograph of NSW-2012 VLPs at 64,000× magnification. The blue and green arrows
370 show examples of VLPs measuring ~46 nm and ~50 nm, respectively. The scale bar
371 represents 100 nm. B) 2D classification of GII.4 NSW-2012 T=4 VLPs. (C) Gold
372 standard FSC plot of the icosahedral reconstruction of NSW-2012 indicates a
373 resolution of 7.3-Å.

374

375 **Figure 4. Cryo-EM reconstruction structure of NSW-2012 T=4 VLPs.** The left
376 side shows NSW-2012 VLPs have a T=4 icosahedral symmetry (symmetry axis

377 labeled 2, 3, and 5). These VLPs were composed of 240 copies of VP1 and VP1
378 adapted four quasiequivalent conformations (A, B, C, and D) that gave rise to two
379 distinct dimers (A/B and C/D). At the icosahedral twofold axis, the B, C, and D
380 subunits were alternating, while the A subunits are positioned at the fivefold axis. The
381 right side shows a cutaway section of these VLPs and indicates that the inner and
382 outer diameters are 32 nm and 50 nm, respectively. The P domains are elevated ~21 Å
383 off the S domain.
384
385 **Figure 5. NSW-2012 T=4 VLPs shows several new structural features.** The cavity
386 and flap-like structures are observed at the twofold axis and are found on opposing
387 sides. The cavity and flap-like structures are associated with the S domain on the D
388 subunit.
389
390 **Figure 6. NSW-2012 T=4 VLPs are formed with 60 A/B and 60 C/D VP1 dimers.**
391 The A/B and C/D dimers show an equivalent convex conformation of the S domain.
392 An additional connection was also observed between the D subunit of the S and P
393 domain.
394
395 **Figure 7. The X-ray crystal structures of NSW-2012 P domain and GI.1 S**
396 **domain were fitted into the T=4 VLP density map.** (A) The X-ray crystal structure
397 of NSW-2012 P domain (4OOS, cartoon) could be fitted into the A/B and C/D P
398 domain dimers, indicating little conformational change. (B) The X-ray crystal
399 structure of the GI.1 S domain (1IHM, cartoon) fitted into the A/B and C/D S domain
400 dimers. However, the cavity and flap-like structures on the D subunit suggests a large
401 conformational change compared to typical T=3 particles.

Figure 8. A close-up view of NSW-2012 C/D dimer. The fitted X-ray crystal structures of the GI.1 S domain (cartoon) and the GII.4 P domain (cartoon) into the cryo-EM map shows the how the hinge region connects the S and P domains. Also, the new connection between the S domain and the C-terminus of the P domain is shown. The asterisk represents the missing hinge region on the X-ray crystal structures that connects of the S and P domains for the C subunit (blue) and D subunit (red).

Figure 9. Cryo-EM reconstruction structure of NSW-2012 T=3 VLPs. (A) 2D classification of 1780 manually picked particles. The first class (red circle) shows particles of a smaller diameter, compared to averages of other classes. These smaller particles were used for further refinement. (B) FSC plot of the icosahedral reconstruction of T=3 VLPs indicates a resolution of 15-Å. (C) The left side shows NSW-2012 exhibiting T=3 icosahedral symmetry (symmetry axis labeled 2, 3, and 5). These VLPs were composed of 180 copies of VP1 that forms A/B and C/C dimers. The cutaway section (right) shows the inner and outer diameter of the particle, which measured 24 and 46 nm, respectively. At this resolution the hinge region could not be resolved, but the large gap between S and P domain indicates that the P domains are raised up from the shell.

Figure 10. CHDC-1974 cryo-EM data processing. (A) A representative cryo-EM micrograph of CHDC-1974 VLPs at 64,000× magnification. The scale bar represents 100 nm. (B) 2D classification of CHDC-1974 particles. (C) FSC plot of the

426 icosahedral reconstruction of CHDC-1974 indicates a resolution of 6.1-Å at 0.143
427 cutoff.
428
429 **Figure 11. Cryo-EM structure and analysis of CHDC-1974 VLPs.** The image on
430 the left side shows that CHDC-1974 VLPs has a T=4 icosahedral symmetry
431 (symmetry axis labeled 2, 3, and 5) and was composed of 240 copies of VP1. The
432 VP1 exhibited four quasiequivalent conformations (A, B, C, and D) that gave rise to
433 two distinct dimers (A/B and C/D). At the icosahedral twofold axis, the B, C, and D
434 subunits were alternating, while the A subunit was located around the fivefold axis.
435 The right side shows a cutaway section of these VLPs and indicates that the inner and
436 outer diameters are 32 nm and 50 nm, respectively. The P domains are elevated ~21 Å
437 off the S domain.
438
439 **Figure 12. CHDC-1974 T=4 VLPs shows several new structural features.** The
440 cavity and flap-like structures are observed at the twofold axis and are found on
441 opposing sides. The cavity and flap-like structures are associated with the S domain
442 on the D subunit.
443
444 **Figure 13. CHDC-1974 T=4 VLPs are formed with 60 A/B and 60 C/D VP1**
445 **dimers.** The A/B and C/D dimers show an equivalent convex confirmation on the S
446 domain. Also, the additional connection between the D subunit of the S and P domain
447 was found on the CHDC-1974 T=4 VLPs.
448
449 **Figure 14. The X-ray crystal structures of CHDC-1974 P domain and GI.1 S**
450 **domain were fitted into the VLP density map.** (A) The X-ray crystal structure of

NSW-2012 P domain (5IYN, cartoon) easily fitted into the A/B and C/D P domain dimer densities. (B) The X-ray crystal structure of the GI.1 S domain (1IHM, cartoon) fitted into the A/B and C/D S domain dimers. However, the cavity and flap-like structures on the D subunit suggests a large conformational change from typical T=3 particles.

Figure 15. A close-up view of CHDC-1974 C/D dimer. The fitted X-ray crystal structures of the GI.1 S domain (cartoon) and the GII.4 P domain (cartoon) into the cryo-EM map shows the how the hinge region connects the S and P domains. Also, the new connection between the S domain and the C-terminus of the P domain is shown. The asterisk represents the missing hinge region on the X-ray crystal structures that connects of the S and P domains for the C subunit (blue) and D subunit (red).

Figure 16. EM images of GII.4 virions. Negative stain EM images of GII.4 virions show that the virions exhibit a smaller diameter (~44 nm) than GII.4 VLPs expressed in insect cells that were ~52 nm (see Figure 2).

468 REFERENCES

469

470 1. **Pogan R, Schneider C, Reimer R, Hansman G, Uetrecht C.** 2018.
471 Norovirus-like VP1 particles exhibit isolate dependent stability profiles.
472 Journal of physics. Condensed matter : an Institute of Physics journal
473 **30:**064006.
474 2. **Hansman GS, Natori K, Shirato-Horikoshi H, Ogawa S, Oka T,**
475 **Katayama K, Tanaka T, Miyoshi T, Sakae K, Kobayashi S, Shinohara**
476 **M, Uchida K, Sakurai N, Shinozaki K, Okada M, Seto Y, Kamata K,**
477 **Nagata N, Tanaka K, Miyamura T, Takeda N.** 2006. Genetic and
478 antigenic diversity among noroviruses. The Journal of general virology
479 **87:**909-919.
480 3. **Donaldson EF, Lindesmith LC, Lobue AD, Baric RS.** 2008. Norovirus
481 pathogenesis: mechanisms of persistence and immune evasion in human
482 populations. Immunol Rev **225:**190-211.
483 4. **Choi SC, Simhadri VR, Tian L, Gil-Krzewska A, Krzewski K, Borrego F,**
484 **Coligan JE.** 2011. Cutting edge: mouse CD300f (CMRF-35-like molecule-1)
485 recognizes outer membrane-exposed phosphatidylserine and can
486 promote phagocytosis. Journal of immunology **187:**3483-3487.
487 5. **Ettayebi K CS, Murakami K, Broughman JR, Karandikar U, Tenge VR,**
488 **Neill FH, Blutt SE, Zeng X, Qu L, Kou B, Opekun AR, Burrin D, Graham**
489 **DY, Ramani S, Atmar RL, Estes MK.** 2016. Replication of human
490 noroviruses in stem cell–derived human enteroids Science **353:**1387-
491 1393.
492 6. **Jones MK, Watanabe M, Zhu S, Graves CL, Keyes LR, Grau KR,**
493 **Gonzalez-Hernandez MB, Iovine NM, Wobus CE, Vinje J, Tibbetts SA,**
494 **Wallet SM, Karst SM.** 2014. Enteric bacteria promote human and mouse
495 norovirus infection of B cells. Science **346:**755-759.
496 7. **Hansman GS, Taylor DW, McLellan JS, Smith TJ, Georgiev I, Tame JR,**
497 **Park SY, Yamazaki M, Gondaira F, Miki M, Katayama K, Murata K,**
498 **Kwong PD.** 2012. Structural basis for broad detection of genogroup II
499 noroviruses by a monoclonal antibody that binds to a site occluded in the
500 viral particle. Journal of virology **86:**3635-3646.
501 8. **Prasad BV, Hardy ME, Dokland T, Bella J, Rossmann MG, Estes MK.**
502 1999. X-ray crystallographic structure of the Norwalk virus capsid.
503 Science **286:**287-290.
504 9. **Lawton JA, Zeng CQ, Mukherjee SK, Cohen J, Estes MK, Prasad BV.**
505 1997. Three-dimensional structural analysis of recombinant rotavirus-
506 like particles with intact and amino-terminal-deleted VP2: implications
507 for the architecture of the VP2 capsid layer. Journal of virology **71:**7353-
508 7360.
509 10. **Prasad BV, Rothnagel R, Jiang X, Estes MK.** 1994. Three-dimensional
510 structure of baculovirus-expressed Norwalk virus capsids. Journal of
511 virology **68:**5117-5125.
512 11. **Lindesmith LC, Costantini V, Swanstrom J, Debbink K, Donaldson EF,**
513 **Vinje J, Baric RS.** 2013. Emergence of a norovirus GII.4 strain correlates

with changes in evolving blockade epitopes. Journal of virology **87:**2803-2813.

12. **Lindesmith LC, Debbink K, Swanstrom J, Vinje J, Costantini V, Baric RS, Donaldson EF.** 2012. Monoclonal antibody-based antigenic mapping of norovirus GII.4-2002. Journal of virology **86:**873-883.
13. **Lindesmith LC, Donaldson EF, Baric RS.** 2011. Norovirus GII.4 strain antigenic variation. Journal of virology **85:**231-242.
14. **Ajami NJ, Barry MA, Carrillo B, Muhaxhiri Z, Neill FH, Prasad BV, Opekun AR, Gilger MA, Graham DY, Atmar RL, Estes MK.** 2012. Antibody responses to norovirus genogroup GI.1 and GII.4 proteases in volunteers administered Norwalk virus. Clinical and vaccine immunology : CVI **19:**1980-1983.
15. **Bok K, Abente EJ, Realpe-Quintero M, Mitra T, Sosnovtsev SV, Kapikian AZ, Green KY.** 2009. Evolutionary dynamics of GII.4 noroviruses over a 34-year period. Journal of virology **83:**11890-11901.
16. **Baric RS, Yount B, Lindesmith L, Harrington PR, Greene SR, Tseng FC, Davis N, Johnston RE, Klapper DG, Moe CL.** 2002. Expression and self-assembly of norwalk virus capsid protein from venezuelan equine encephalitis virus replicons. Journal of virology **76:**3023-3030.
17. **Hutson AM, Robert L. Atmar, David Y. Graham, and Mary K. Estes. .** 2002. Norwalk virus infection and disease is associated with ABO histo-blood group type. Journal of Infectious Diseases **185:**1335-1337.
18. **Marionneau S, Ruvoën N, Le Moullac–Vaidye B, Clement M, Cailleau–Thomas A, Ruiz–Palacois G, Huang P, Jiang X, Le Pendu J.** 2002. Norwalk virus binds to histo-blood group antigens present on gastroduodenal epithelial cells of secretor individuals. Gastroenterology **122:**1967-1977.
19. **Tan M, Jiang X.** 2005. The p domain of norovirus capsid protein forms a subviral particle that binds to histo-blood group antigen receptors. Journal of virology **79:**14017-14030.
20. **Tan M, Huang P, Meller J, Zhong W, Farkas T, Jiang X.** 2003. Mutations within the P2 domain of norovirus capsid affect binding to human histo-blood group antigens: evidence for a binding pocket. Journal of virology **77:**12562-12571.
21. **Kilic T, Koromyslova A, Hansman GS.** 2019. Structural Basis for Human Norovirus Capsid Binding to Bile Acids. Journal of virology **93**.
22. **Ettayebi K, Crawford SE, Murakami K, Broughman JR, Karandikar U, Tenge VR, Neill FH, Blutt SE, Zeng XL, Qu L, Kou B, Opekun AR, Burrin D, Graham DY, Ramani S, Atmar RL, Estes MK.** 2016. Replication of human noroviruses in stem cell-derived human enteroids. Science **353:**1387-1393.
23. **Bhella D, Goodfellow IG.** 2011. The cryo-electron microscopy structure of feline calicivirus bound to junctional adhesion molecule A at 9-angstrom resolution reveals receptor-induced flexibility and two distinct conformational changes in the capsid protein VP1. Journal of virology **85:**11381-11390.
24. **Chen R, Neill JD, Noel JS, Hutson AM, Glass RI, Estes MK, Prasad BV.** 2004. Inter- and intragenus structural variations in caliciviruses and their functional implications. Journal of virology **78:**6469-6479.

25. **Kilic T, Koromyslova A, Malak V, Hansman GS.** 2018. Atomic Structure of the Murine Norovirus Protruding Domain and Soluble CD300lf Receptor Complex. Journal of virology **92**.
26. **Melgaco FG, Correa AA, Ganime AC, Brandao MLL, Medeiros VM, Rosas CO, Lopes S, Miagostovich MP.** 2018. Evaluation of skimmed milk flocculation method for virus recovery from tomatoes. Brazilian journal of microbiology : [publication of the Brazilian Society for Microbiology].
27. **Forest KT, Filutowicz MS.** 2003. Remodeling of replication initiator proteins. Nature structural biology **10:**496-498.
28. **Eden JS, Tanaka MM, Boni MF, Rawlinson WD, White PA.** 2013. Recombination within the pandemic norovirus GII.4 lineage. Journal of virology **87:**6270-6282.
29. **Hansman GS, Natori K, Oka T, Ogawa S, Tanaka K, Nagata N, Ushijima H, Takeda N, Katayama K.** 2005. Cross-reactivity among sapovirus recombinant capsid proteins. Archives of virology **150:**21-36.
30. **Hansman GS, Saito H, Shibata C, Ishizuka S, Oseto M, Oka T, Takeda N.** 2007. Outbreak of gastroenteritis due to sapovirus. Journal of clinical microbiology **45:**1347-1349.
31. **Koromyslova AD, Hansman GS.** 2017. Nanobodies targeting norovirus capsid reveal functional epitopes and potential mechanisms of neutralization. PLoS pathogens **13:**e1006636.
32. **Pyrkov TV, Chugunov AO, Krylov NA, Nolde DE, Efremov RG.** 2009. PLATINUM: a web tool for analysis of hydrophobic/hydrophilic organization of biomolecular complexes. Bioinformatics **25:**1201-1202.
33. **McCoy AJ G-KR, Adams PD, Winn MD, Storoni LC, Read RJ. .** 2007. Phaser crystallographic software. Journal of Applied Crystallography. **40:**658-674.
34. **Kabsch W.** 2010. XDS. Acta Cryst. **D66:**125-132.
35. **Sedji MI, Varbanov M, Meo M, Colin M, Mathieu L, Bertrand I.** 2018. Quantification of human adenovirus and norovirus in river water in the north-east of France. Environmental science and pollution research international.
36. **Emsley P LB, Scott WG, Cowtan K.** 2010. Features and development of Coot. Acta Crystallographica Section D: Biological Crystallography. **66:**486-501.
37. **Singh BK, Leuthold MM, Hansman GS.** 2015. Human noroviruses' fondness for histo-blood group antigens. Journal of virology **89:**2024-2040.
38. **Bertolotti-Ciarlet A, White LJ, Chen R, Prasad BV, Estes MK.** 2002. Structural requirements for the assembly of Norwalk virus-like particles. Journal of virology **76:**4044-4055.
39. **Koromyslova AD, Hansman GS.** 2015. Nanobody binding to a conserved epitope promotes norovirus particle disassembly. Journal of virology **89:**2718-2730.
40. **Koromyslova AD, Morozov VA, Hefele L, Hansman GS.** 2018. Human Norovirus Neutralized by a Monoclonal Antibody Targeting the HBGA Pocket. Journal of virology.

41. **Doerflinger SY, Tabatabai J, Schnitzler P, Farah C, Rameil S, Sander P, Koromyslova A, Hansman GS.** 2016. Development of a Nanobody-Based Lateral Flow Immunoassay for Detection of Human Norovirus. mSphere **1**.
42. **Parra GI, Bok K, Taylor R, Haynes JR, Sosnovtsev SV, Richardson C, Green KY.** 2012. Immunogenicity and specificity of norovirus Consensus GII.4 virus-like particles in monovalent and bivalent vaccine formulations. Vaccine **30:**3580-3586.
43. **Clayton JS, Bolinger HK, Jaykus LA.** 2018. Disinfectant testing against human norovirus surrogates-What infection preventionists need to know. Infection control and hospital epidemiology**:**1-2.
44. **Bernstein DI, Atmar RL, Lyon GM, Treanor JJ, Chen WH, Jiang X, Vinje J, Gregoricus N, Frenck RW, Jr., Moe CL, Al-Ibrahim MS, Barrett J, Ferreira J, Estes MK, Graham DY, Goodwin R, Borkowski A, Clemens R, Mendelman PM.** 2015. Norovirus vaccine against experimental human GII.4 virus illness: a challenge study in healthy adults. The Journal of infectious diseases **211:**870-878.
45. **Koromyslova A, Tripathi S, Morozov V, Schroten H, Hansman GS.** 2017. Human norovirus inhibition by a human milk oligosaccharide. Virology **508:**81-89.
46. **Hansman GS, Doan LT, Kguyen TA, Okitsu S, Katayama K, Ogawa S, Natori K, Takeda N, Kato Y, Nishio O, Noda M, Ushijima H.** 2004. Detection of norovirus and sapovirus infection among children with gastroenteritis in Ho Chi Minh City, Vietnam. Archives of virology **149:**1673-1688.

Figure 1

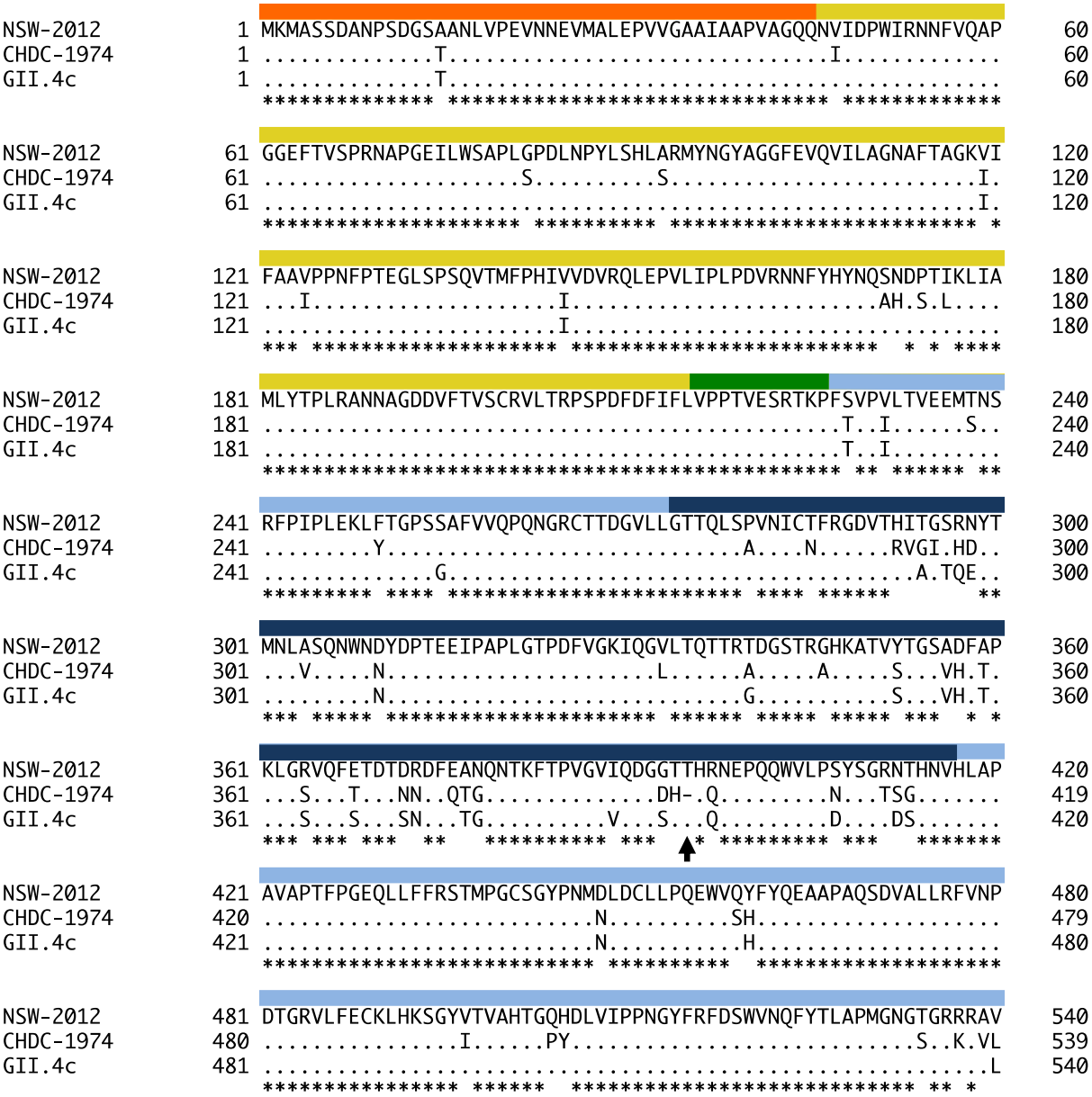
NSW-2012 1 MKMASSDANPSDGSAANLVPEVNNEVMALEPVVGAAIAAPVAGQQNVIDPWIRNNFVQAP 60
CHDC-1974 1 .....T.....I..... 60
GII.4c 1 .....T..... 60
NSW-2012 61 GGEFTVSPRNAPGEILWSAPLGPDLNPYLSHLARMYNGYAGGFEVQVILAGNAFTAGKVI 120
CHDC-1974 61 .....S.....S.....I. 120
GII.4c 61 .....I. 120
NSW-2012 121 FAAVPPNFPTEGLSPSQVTMFPHIVVDVRQLEPVLIPLPDVRNNFYHYNQSNDPTIKLIA 180
CHDC-1974 121 ...I.....I.....AH.S.L.... 180
GII.4c 121 .....I..... 180
NSW-2012 181 MLYTPLRANNAGDDVFTVSCRVLTRPSPDFDFIFLVPPTVESRTKPFSVPVLTVEEMTNS 240
CHDC-1974 181 .....T..I.....S.. 240
GII.4c 181 .....T..I..... 240
NSW-2012 241 RFPIPLEKLFTGPSSAFVVQPQNGRCTTDGVLLGTTQLSPVNICTFRGDVTHITGSRNYT 300
CHDC-1974 241 .....Y.....A....N.....RVGI.HD.. 300
GII.4c 241 .....G.....A.TQE.. 300
NSW-2012 301 MNLASQNWNDYDPTEEIPAPLGTPDFVGKIQGVLTQTTRTDGSTRGHKATVYTGSADFAP 360
CHDC-1974 301 ...V.....N.....L.....A.....A.....S...VH.T. 360
GII.4c 301 .....N.....G.....S...VH.T. 360
NSW-2012 361 KLGRVQFETDTDRDFEANQNTKFTPVGVIQDGGTTHRNEPQQWVLPSYSGRNTHNVHLAP 420
CHDC-1974 361 ...S...T...NN..QTG.....DH-.Q.....N...TSG..... 419
GII.4c 361 ...S...S...SN...TG.....V...S...Q.....D....DS..... 420
NSW-2012 421 AVAPTFPGEQLLFFRSTMPGCSGYPNMDLDCLLPQEWVQYFYQEAAPAQSDVALLRFVNP 480
CHDC-1974 420 .....N.....SH..... 479
GII.4c 421 .....N.....H..... 480
NSW-2012 481 DTGRVLFECKLHKSGYVTVAHTGQHDLVIPPNGYFRFDSWVNQFYTLAPMGNGTGRRRAV 540
CHDC-1974 480 .....I.....PY.....S..K.VL 539
GII.4c 481 .....L 540

Figure 2

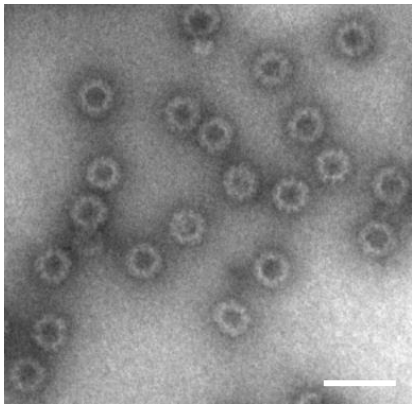

GII.4 NSW-2012

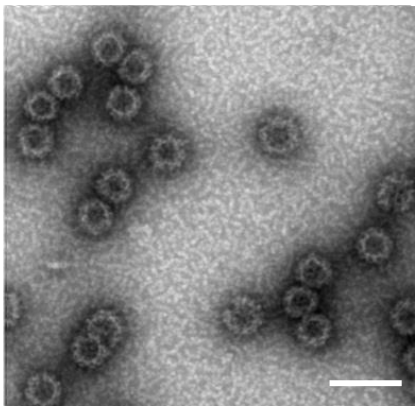

GII.4 CHDC-1974

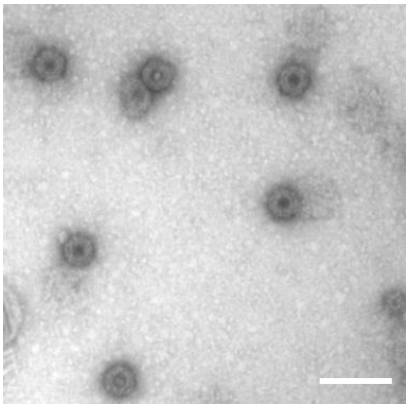

GI.1 West Chester

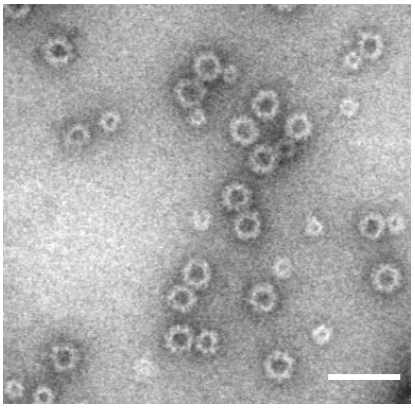

GII.10 026-Vietnam

Figure 3

A

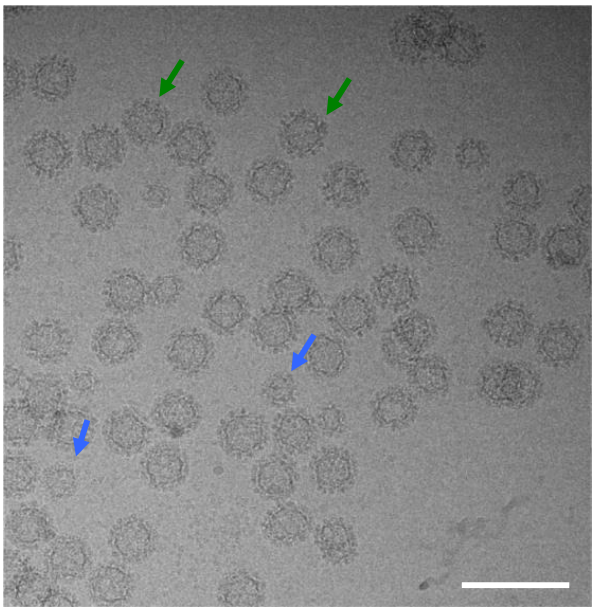

B

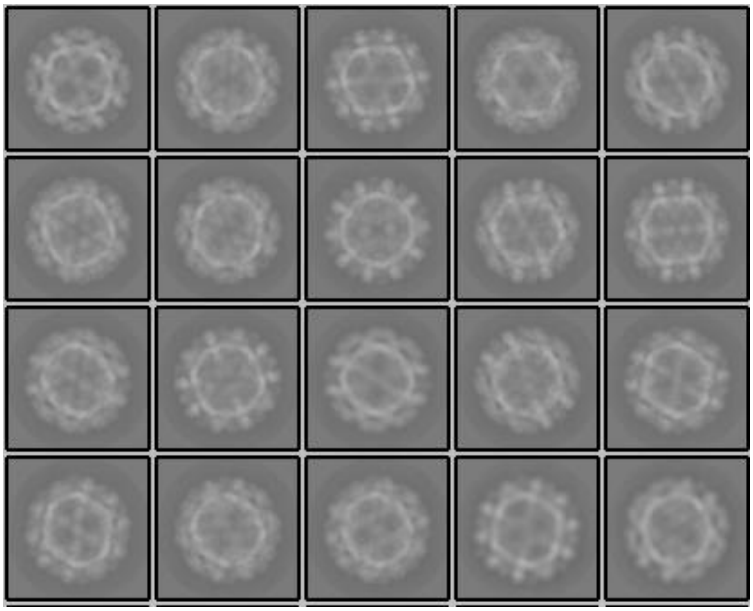

C

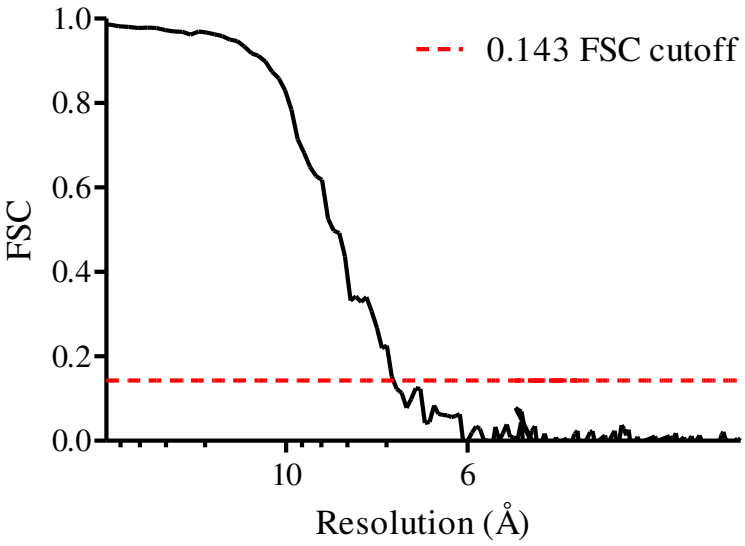

Figure 4

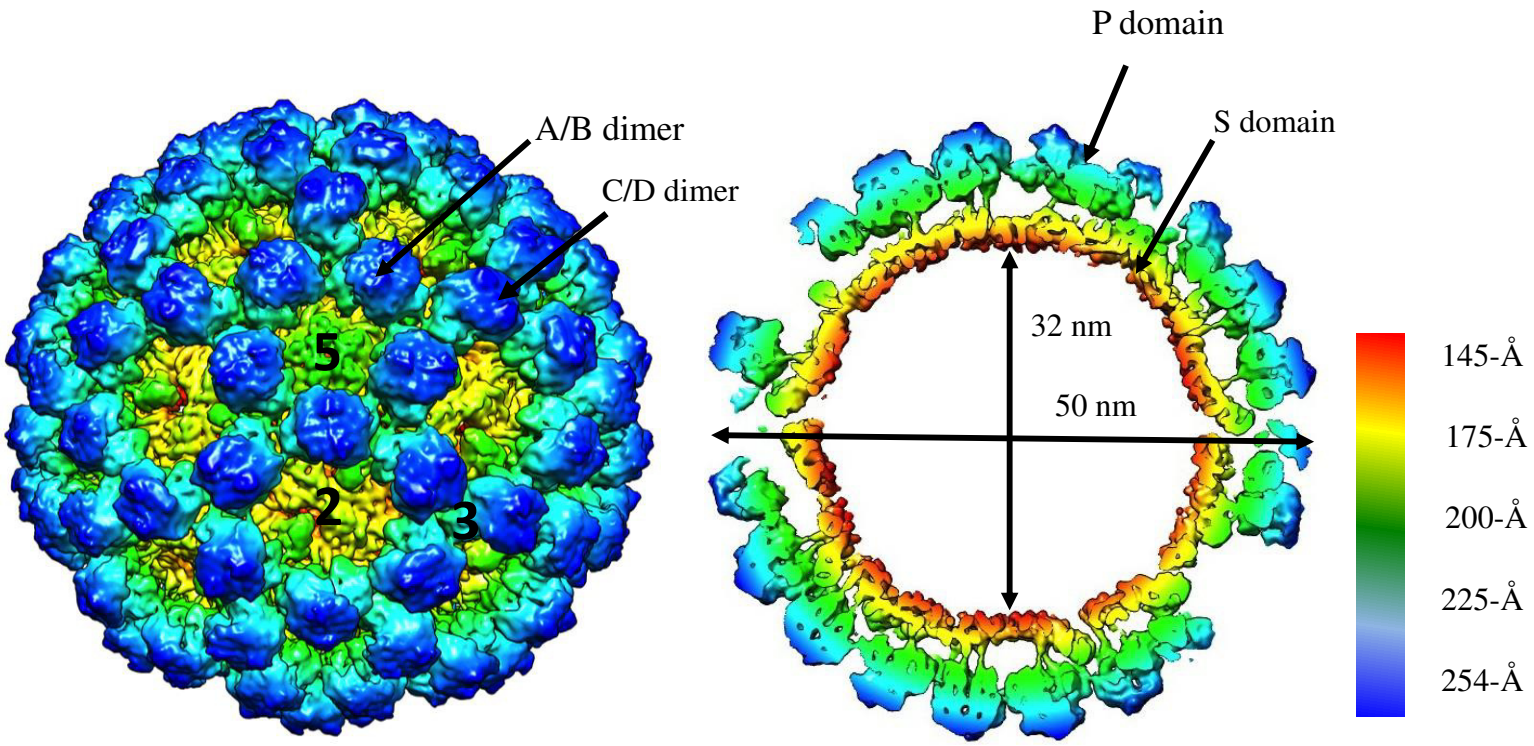
A/B dimer
C/D dimer
5
2
3
P domain
S domain
32 nm
50 nm
145-Å
175-Å
200-Å
225-Å
254-Å

Figure 5

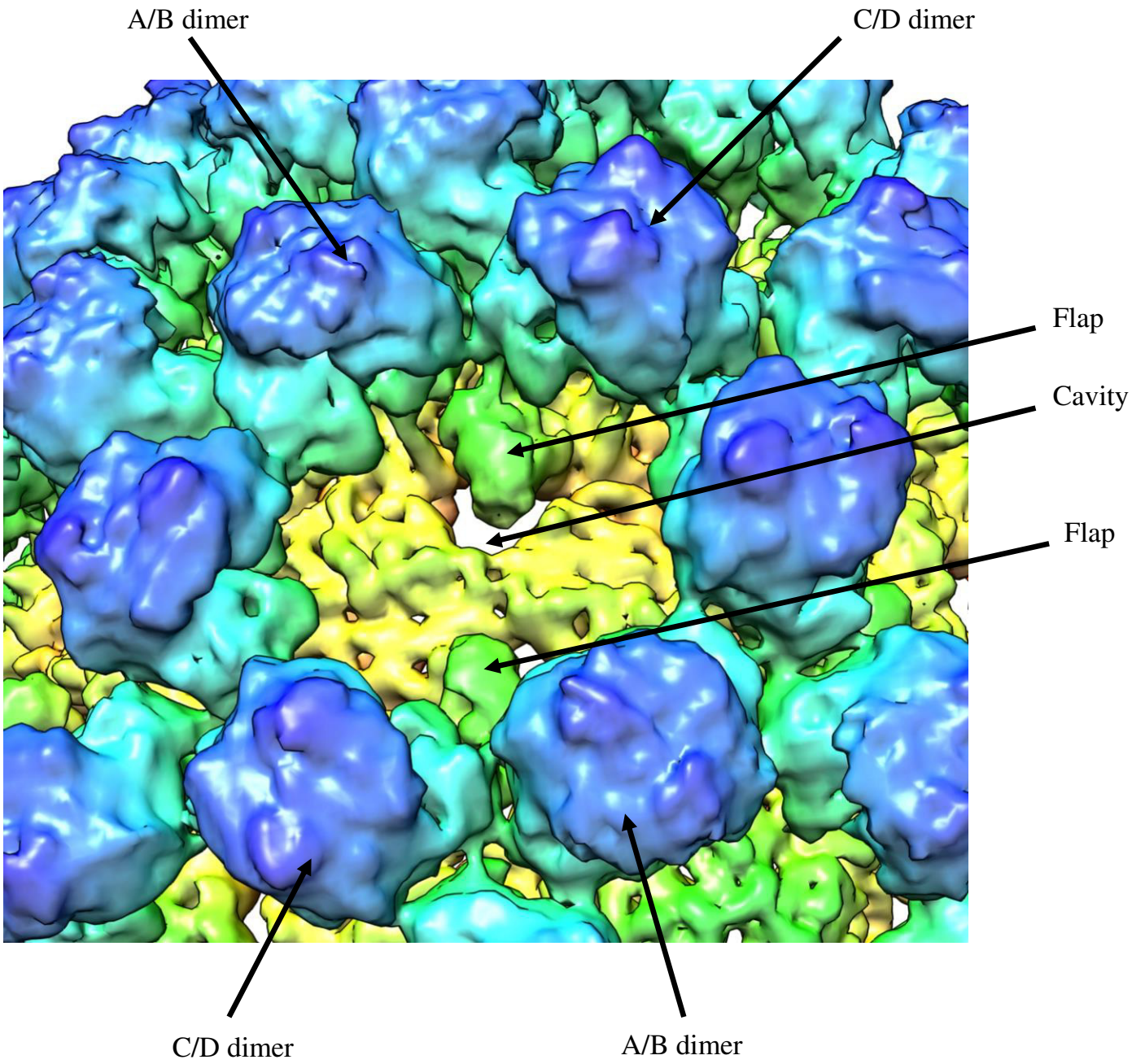

Figure 6

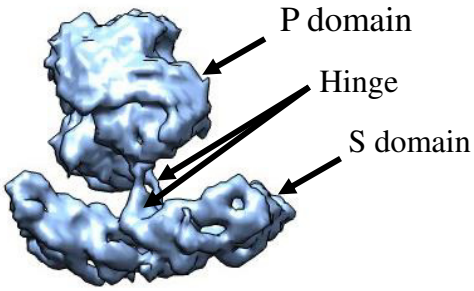

A/B dimer

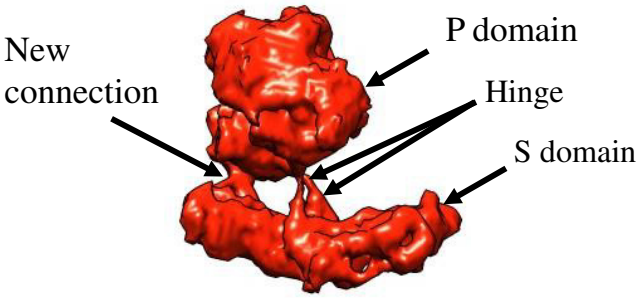

C/D dimer

Figure 7

A

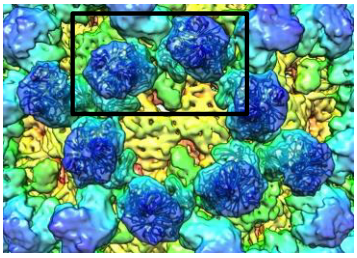

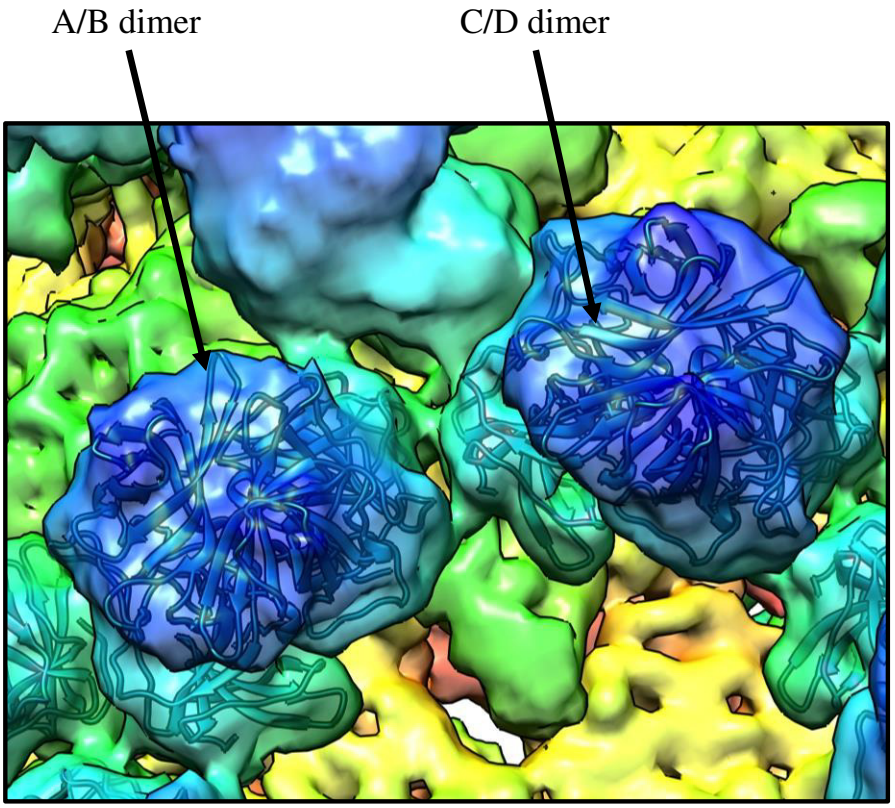

B

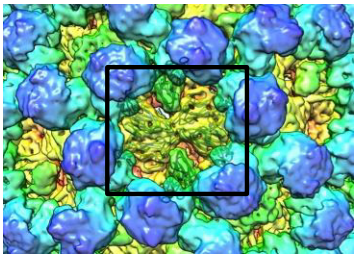

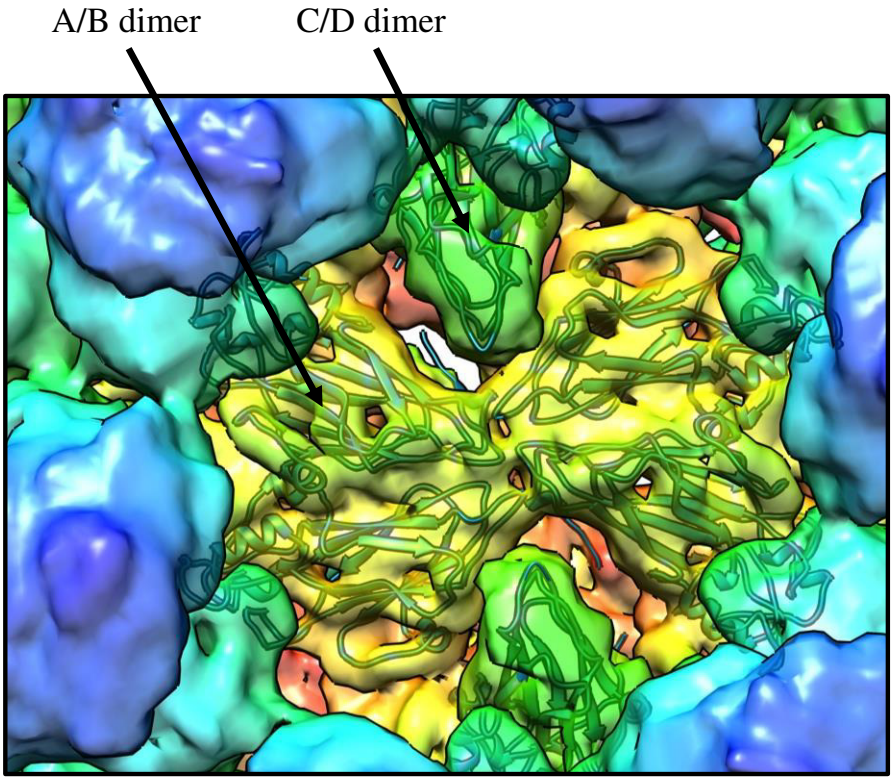

Figure 8

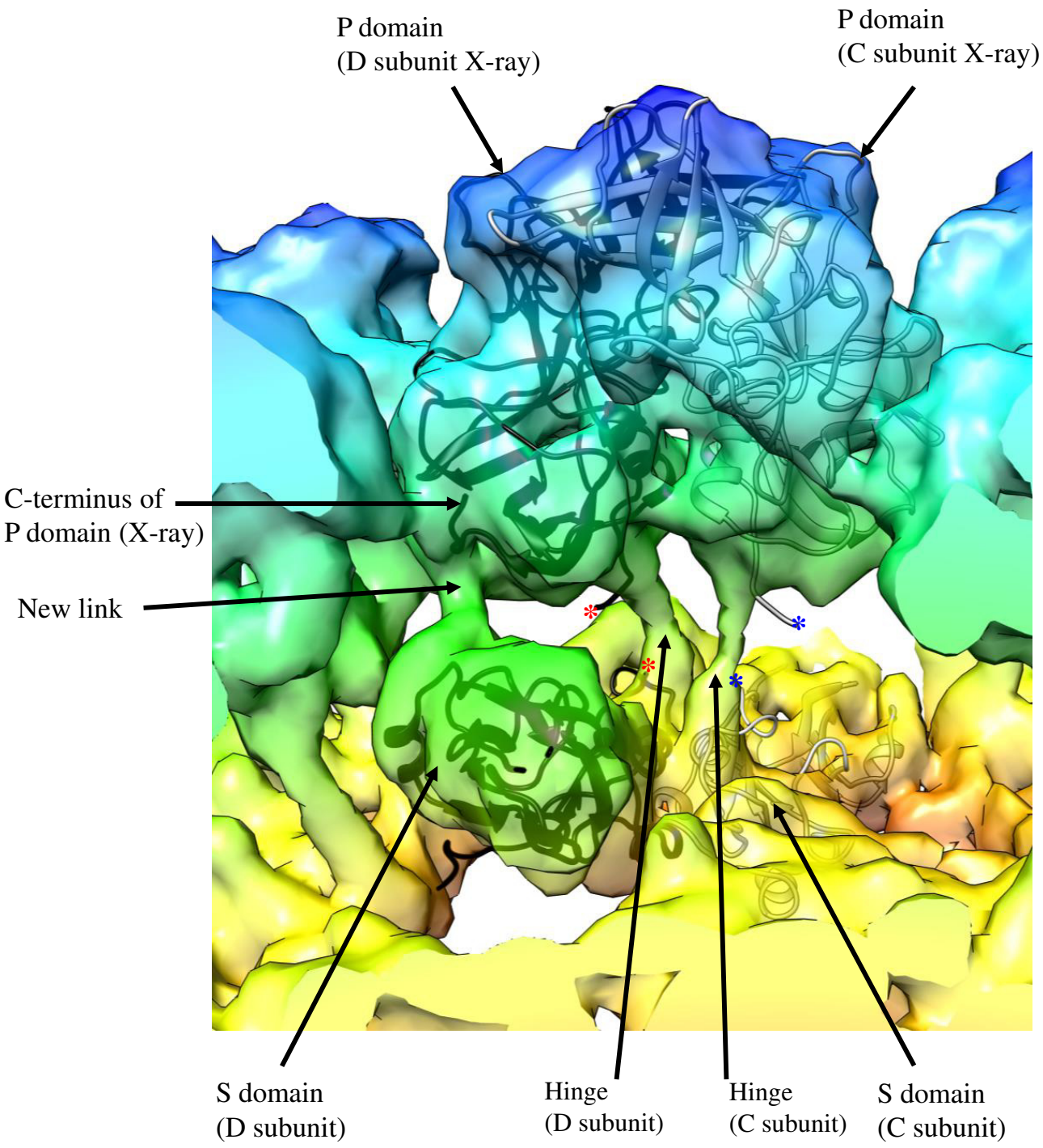
P domain
(D subunit X-ray)
P domain
(C subunit X-ray)
C-terminus of
P domain (X-ray)
New link
S domain
(D subunit)
Hinge
(D subunit)
Hinge
(C subunit)
S domain
(C subunit)

Figure 9

A

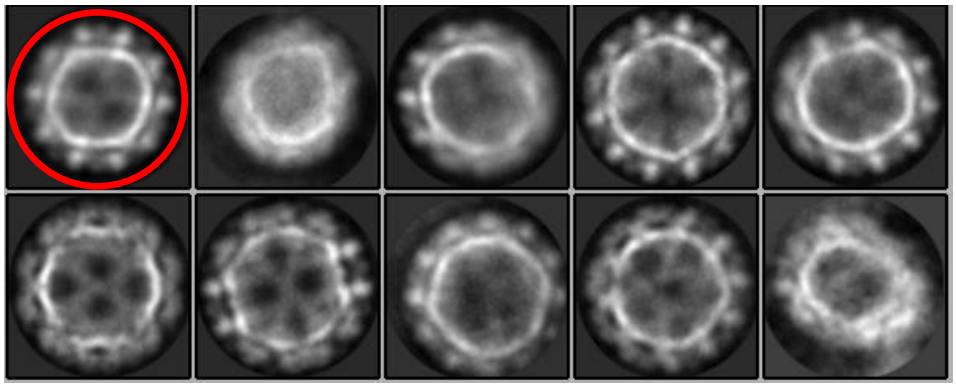

B

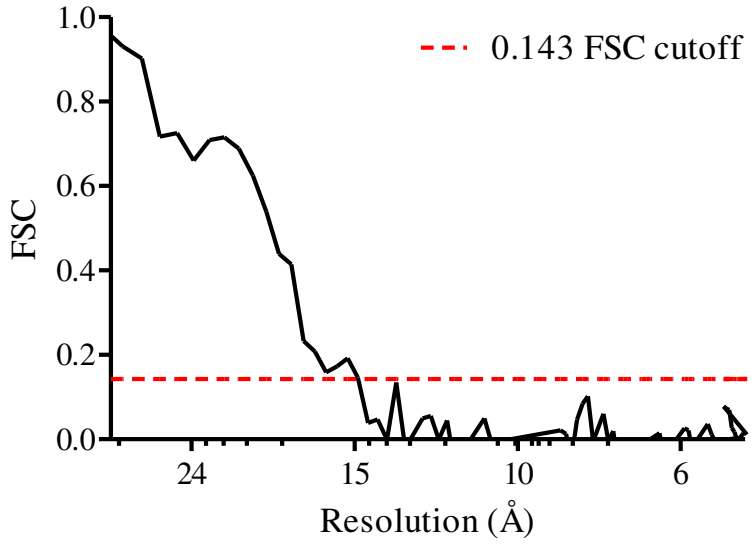
1.0
0.8
0.6
0.4
0.2
0.0
FSC
0.143 FSC cutoff
24
15
10
6
Resolution (Å)

C

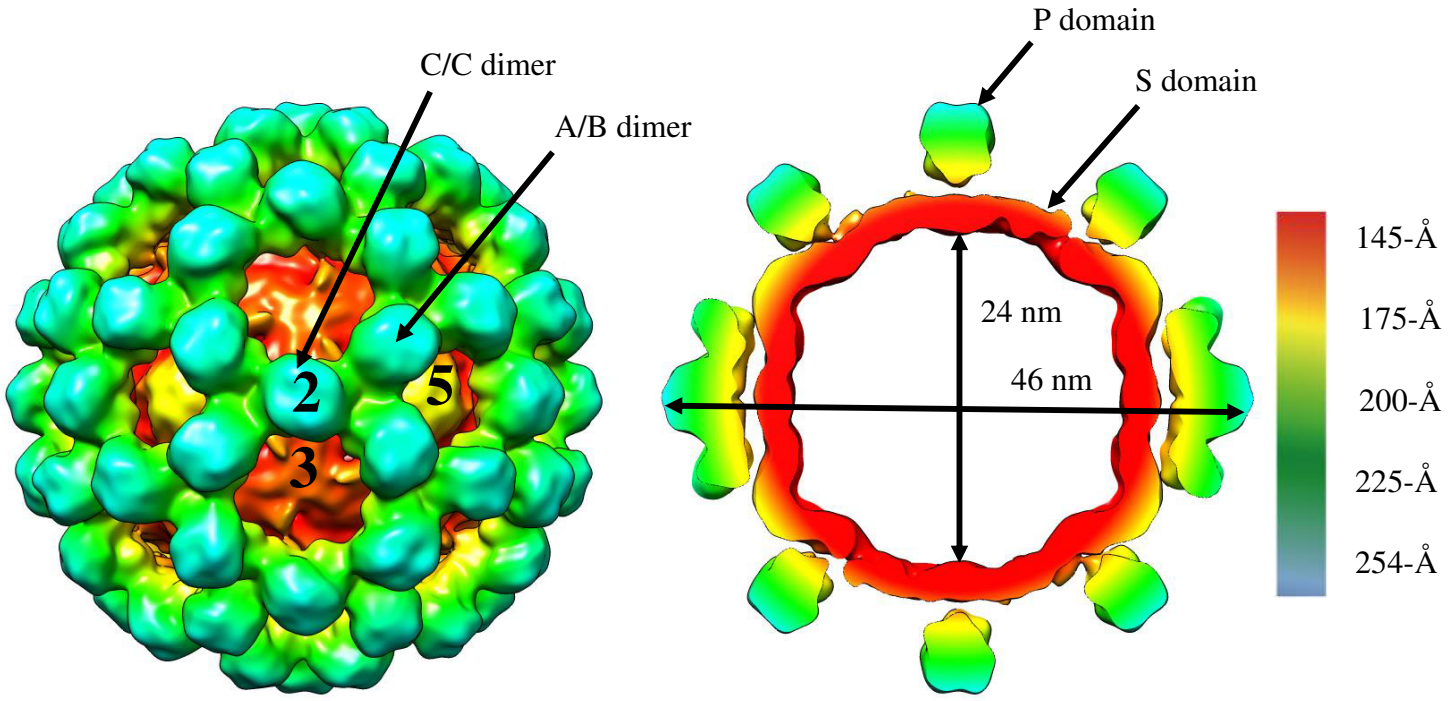
C/C dimer
A/B dimer
2
5
3
P domain
S domain
24 nm
46 nm
145-Å
175-Å
200-Å
225-Å
254-Å

Figure 10

A

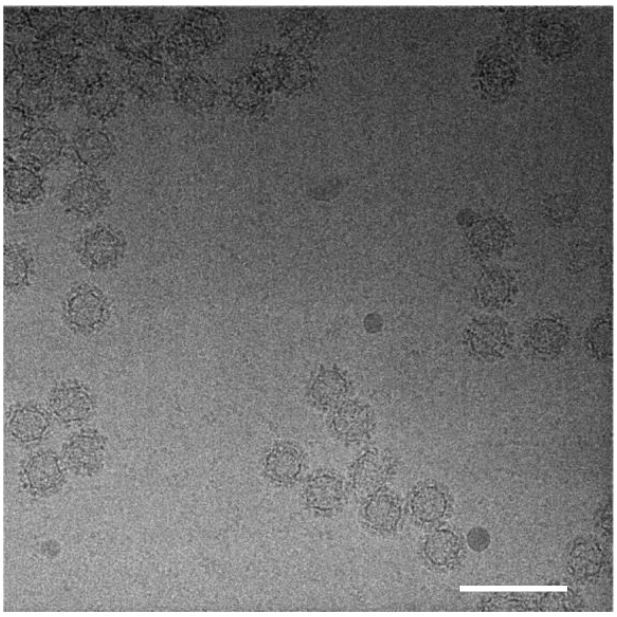

B

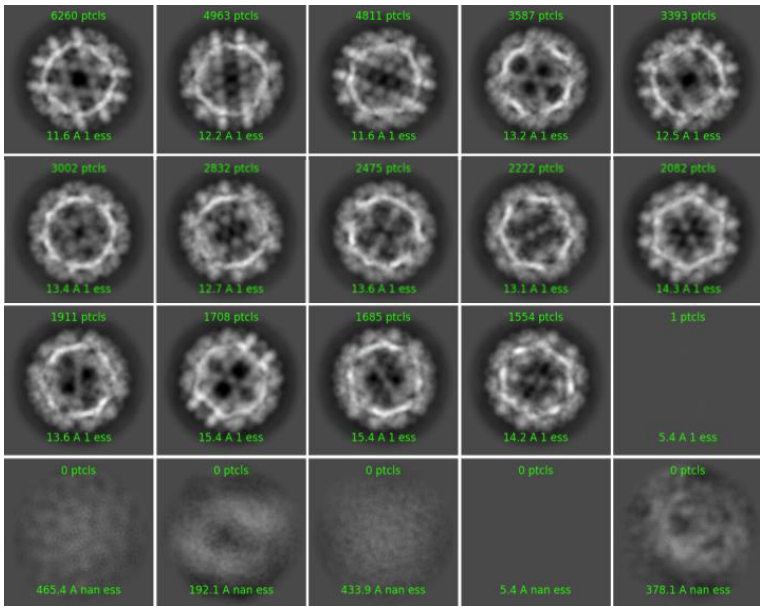

C

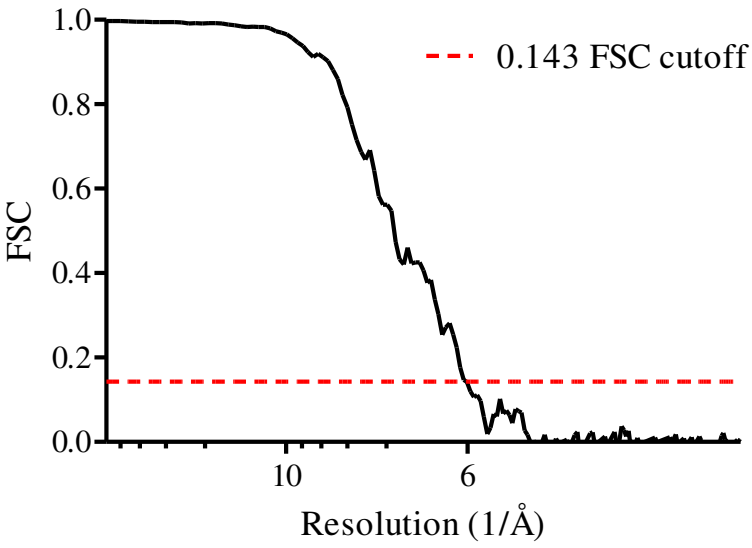

Figure 11

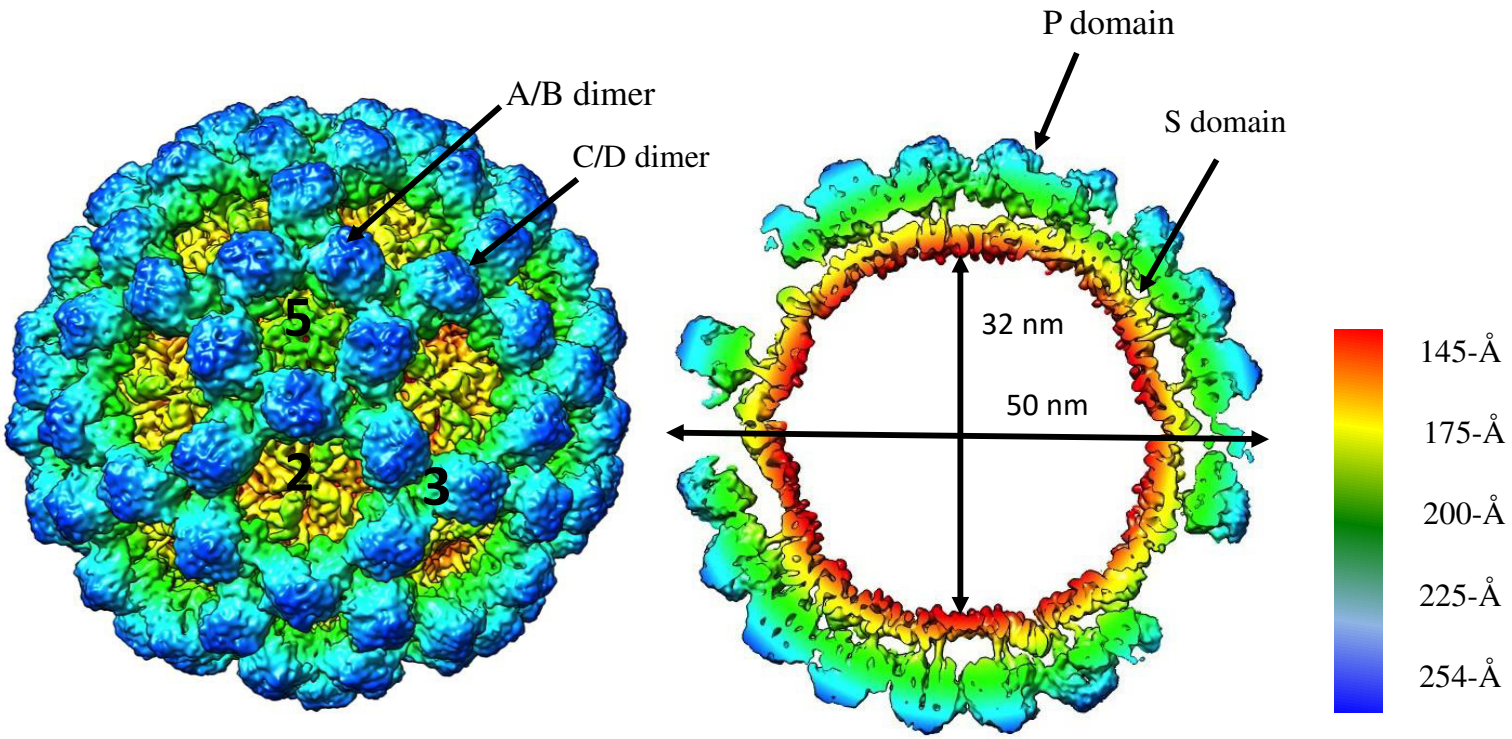
A/B dimer
C/D dimer
5
2
3
P domain
S domain
32 nm
50 nm
145-Å
175-Å
200-Å
225-Å
254-Å

Figure 12

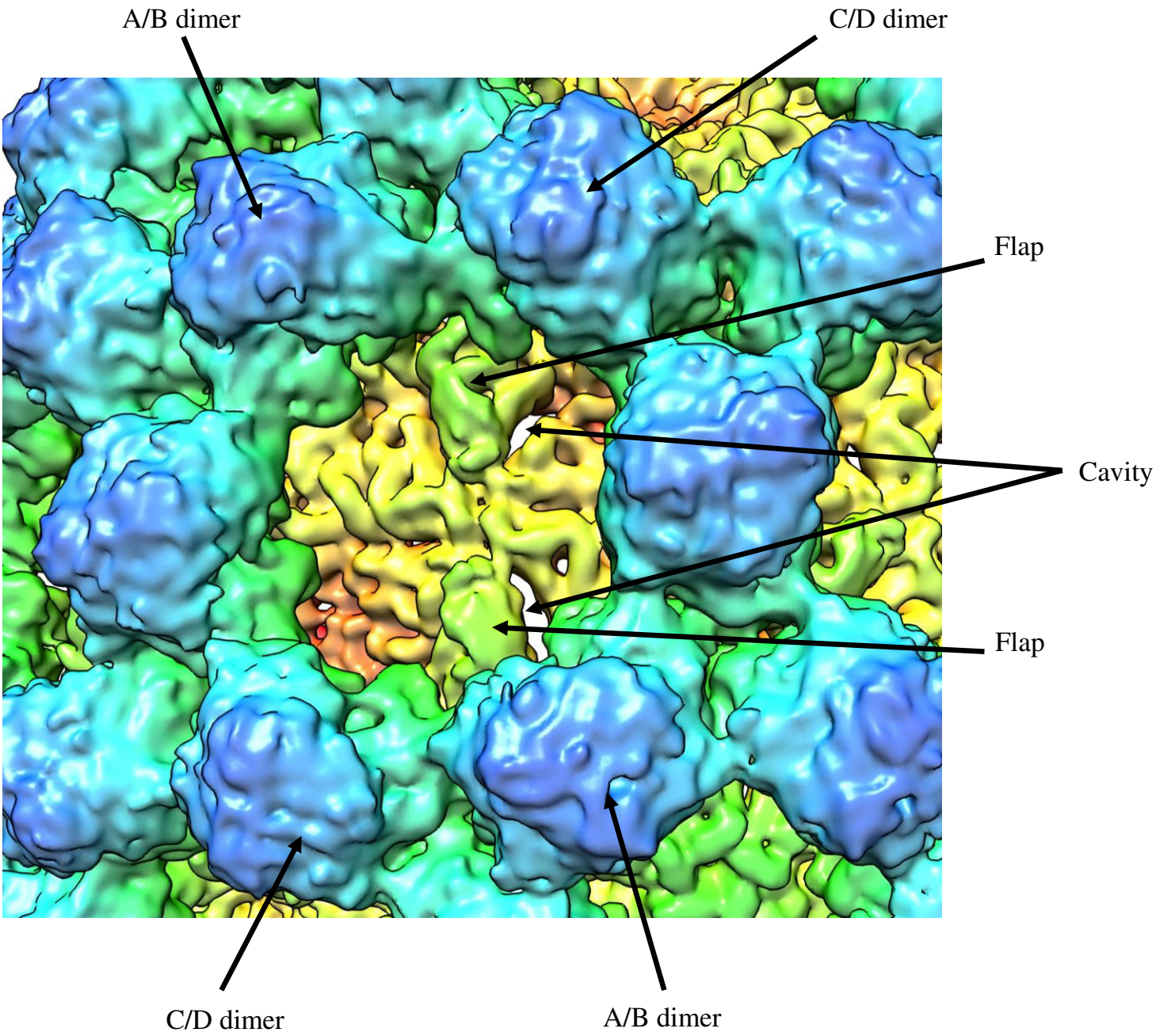

Figure 13

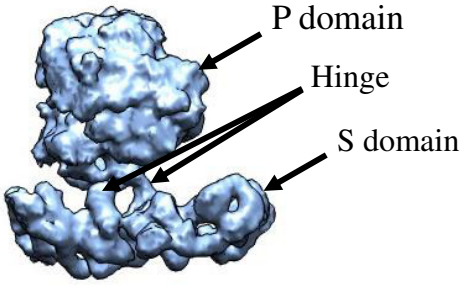

A/B dimer

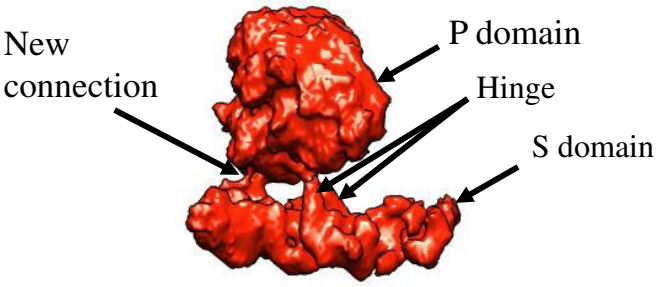

C/D dimer

Figure 14

A

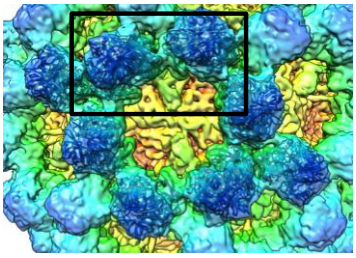

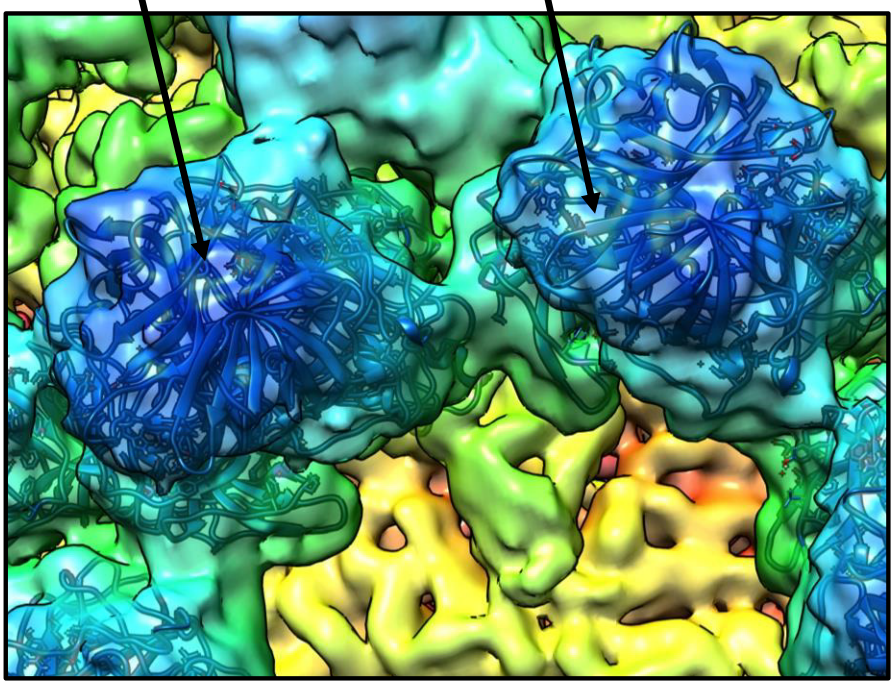

B

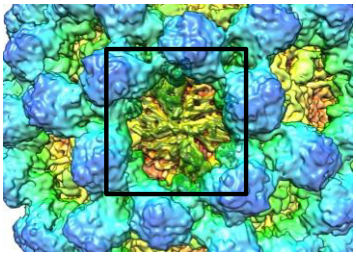

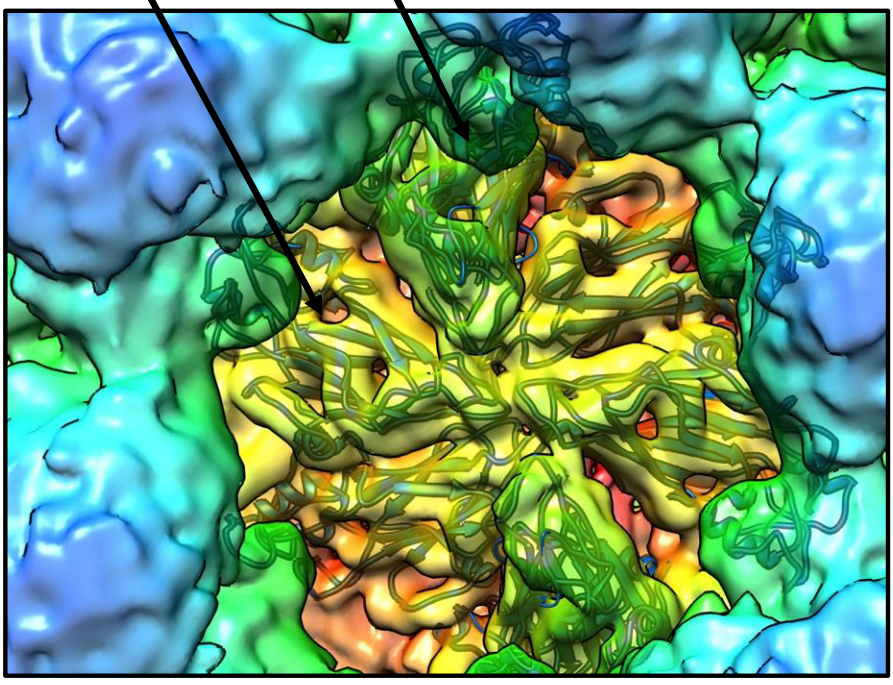

Figure 15

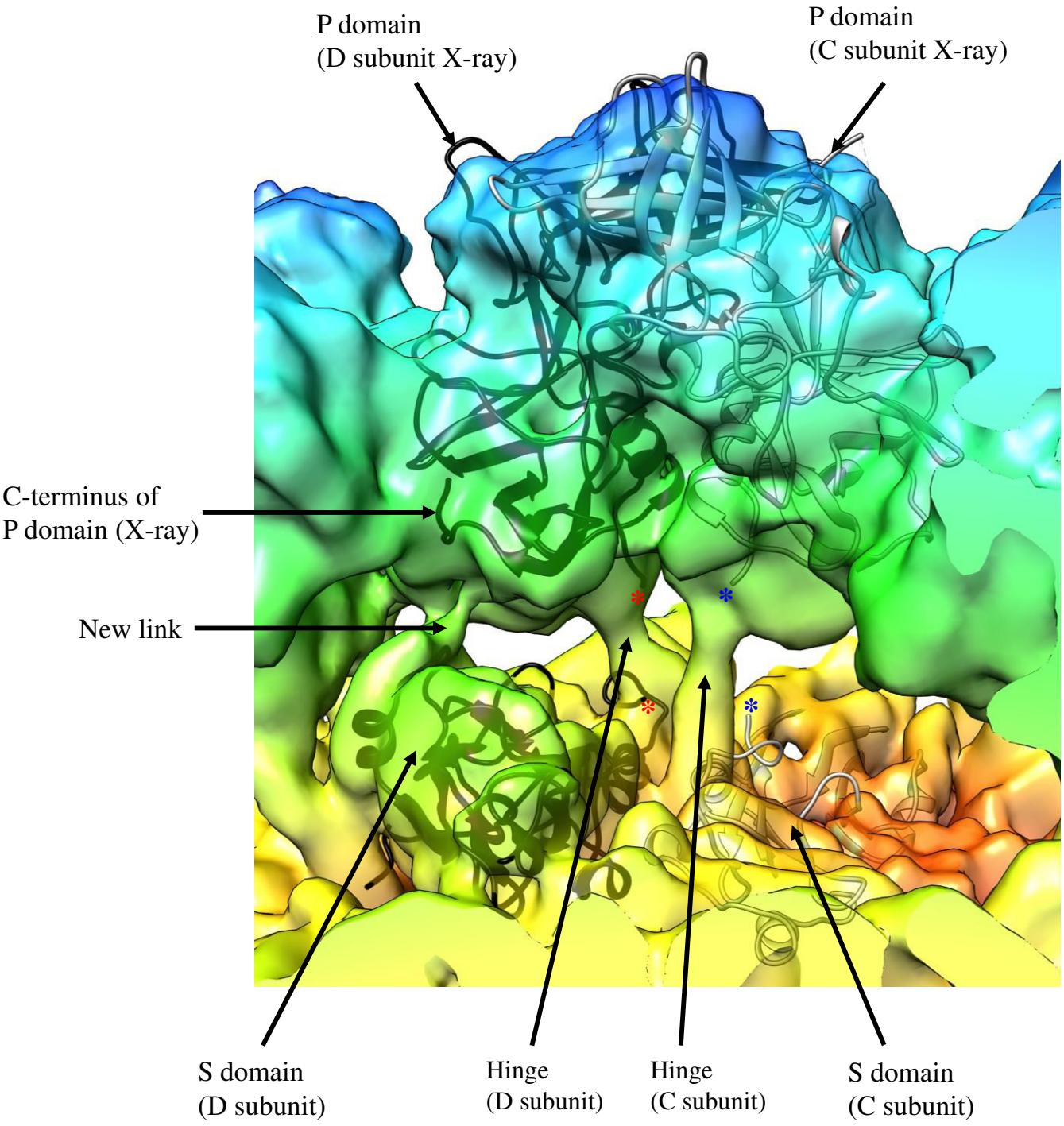
P domain
(D subunit X-ray)
P domain
(C subunit X-ray)
C-terminus of
P domain (X-ray)
New link
S domain
(D subunit)
Hinge
(D subunit)
Hinge
(C subunit)
S domain
(C subunit)

Figure 16